

CHEMISTRY

Metallurgy and high temperature chemistry

INVESTIGATION OF THE SURFACE FEATURES
OF TiO₂/Sm₂O₃ THIN FILMS PREPARED
BY SOL-GEL METHOD

Stancho I. Yordanov[✉], Bojidar T. Jivov, Vladimir P. Petkov,
Yoanna G. Kostova, Vanya L. Dyakova, Mihaela K. Aleksandrova,
Shaban R. Uzun

Received on January 8, 2026

Presented by V. Bankova, Member of BAS, on February 24, 2026

Abstract

Nanostructured TiO₂ thin films doped with Sm₂O₃ were synthesized by the sol-gel method using titanium isopropoxide and titanium butoxide as precursors. The coatings were deposited on 316L stainless steel substrates and investigated with respect to their morphology, structure, and protective efficiency. Cyclic corrosion tests in a 3.5% NaCl solution for 100 h demonstrated excellent protective behaviour. Samples containing 1 at.% Sm in titanium isopropoxide (Sm2) and 0.5 at.% Sm in titanium butoxide (Sm3) exhibited the highest corrosion resistance, with negligible or zero corrosion rates. The results indicate that the incorporation of samarium into sol-gel derived TiO₂ coatings enhances their protective performance and stability in chloride-containing environments, making them promising candidates for advanced anticorrosion applications.

Key words: TiO₂ thin films, sol-gel method, Sm₂O₃ doping, surface morphology, corrosion resistance, potentiodynamic polarization curves (PDC), XRD

Introduction. Under real service conditions, various metal products are subjected to the intensive impact of a number of corrosion factors. This significant

problem affects the activities of various economic sectors [1–3], including construction, industrial production, energy, agriculture, transport, shipping, healthcare, and many others. One of the commonly used approaches to protect metal products from corrosion and other factors is the application of appropriate protective coatings [4–6]. At the same time, the development of new effective anticorrosion coatings that can further extend the service life of materials remains of significant interest [2, 6–8].

Titanium dioxide functional coatings are applicable in various technical industries, such as photocatalytic systems [9], electrochromic displays [10], photosensitized solar cells [11], and many others. As a promising technological possibility, the preparation of resistant anticorrosion protective coatings based on TiO_2 has been widely considered [12, 13]. The performance characteristics of TiO_2 coatings depend to a significant extent on the deposition approach and the applied heat-treatment regime [14].

A suitable technological method for producing thin coatings is the sol–gel technique, which provides a number of advantages [15–18], including higher homogeneity for multicomponent compositions, relatively low synthesis temperatures, stable final-product characteristics, cost-effective yields, low environmental impact, and relatively low equipment and reagent costs.

Two standard technological methods (spin coating and dip coating) are mainly used for the deposition of thin films by the sol–gel technique. During the synthesis of oxide phases by the sol–gel method, several main stages can be distinguished [15–17]: preparation of a solution from suitable precursors; hydrolysis and partial condensation of alkoxides to form a sol; gel formation by polycondensation of the hydrolyzed precursors; evaporation of the solvent during drying and formation of a xerogel; and finally, obtaining stable oxide products after heat treatment.

The main objective of the present article is to study the characteristics of anticorrosion protective coatings deposited by the sol–gel technique, based on TiO_2 modified with Sm_2O_3 . Sm_2O_3 was selected as a dopant because Sm^{3+} ions are known to stabilize sol–gel oxide networks, reduce defect density and porosity, and improve the barrier properties of TiO_2 coatings, resulting in enhanced corrosion resistance.

Materials and methods. Nanostructured TiO_2 coatings doped with samarium were synthesized by the sol–gel method with the aim of enhancing the corrosion resistance of 316L stainless steel. Two organic titanium precursors were employed for the preparation of the deposition sols: titanium isopropoxide (TTIP) and titanium butoxide. Acetylacetonate (AcAc) served as a stabilizing agent.

For the TiO_2 sol preparation, TTIP, titanium butoxide, and AcAc were dissolved in 2-propanol. The obtained solution was clear and orange in colour, indicating the formation of a chelated complex. After vigorous stirring at room temperature, a mixture of distilled water and isopropanol (iPrOH) was added dropwise under continuous stirring. The molar ratio of the components in the

TTIP-based sol was TTIP:iPrOH:H₂O:AcAc = 1:30:1:1. The sol based on titanium butoxide was prepared following the same procedure.

A samarium solution was obtained by dissolving Sm₂O₃ in 2 M nitric acid and isopropanol to a final concentration of 0.1 M. The required volume of samarium solution was added to the titanium sols to prepare four compositions:

- Sm1 – sol containing 0.5 at.% Sm in TTIP-based solution;
- Sm2 – sol containing 1 at.% Sm in TTIP-based solution;
- Sm3 – sol containing 0.5 at.% Sm in titanium butoxide-based solution;
- Sm4 – sol containing 1 at.% Sm in titanium butoxide-based solution.

Atomic force microscopy (AFM) was performed using a NanoScope V system (Bruker Ltd., Germany) operating in tapping mode under ambient conditions. Silicon cantilevers (Tap300Al-G, Budget Sensors, Innovative Solutions Ltd., Bulgaria) with a 30 nm aluminum reflex coating were used. According to the manufacturer's specifications, the cantilevers had a spring constant of 1.5–15 N/m, a resonance frequency of 150 ± 75 kHz, and a tip radius below 10 nm. Images were acquired at a scan rate of 1 Hz in the highest resolution mode (512×512 pixels). NanoScope software was employed for cross-sectional analysis and roughness evaluation.

X-ray diffraction (XRD) analysis was performed using a Philips PW1030 diffractometer in θ – 2θ Bragg–Brentano geometry with CuK α radiation (30 kV, 20 mA) and a wavelength of $\lambda = 1.5406$ Å. The XRD patterns were recorded at room temperature over the 2θ range of 19° – 40° , with a step size of 0.02° . The diffractograms were interpreted using the PDF 2-2022 database (ICDD).

The surface morphology of the coatings was examined by scanning electron microscopy (SEM, HIROX5050) operated at an accelerating voltage of 30 kV in secondary electron mode.

Results and discussion. *Protective properties of the sol–gel coatings.* The protective efficiency of the applied sol–gel coatings was evaluated by cyclic corrosion tests carried out in a 3.5% NaCl medium for a total duration of 100 h. The results demonstrated that the coatings exhibited excellent protective properties. After the completion of the tests, no visible signs of corrosion damage were detected on the coated samples. The surfaces remained smooth, without turbidity or the presence of macroscopic defects.

Among the investigated specimens, samples Sm2 and Sm3 showed the lowest corrosion rates. In particular, after 100 h of testing, sample Sm3 did not exhibit any measurable mass loss, corresponding to a corrosion rate of zero (Table 1). For sample Sm2, no corrosion was observed during the first 50 h, and after 100 h the corrosion rate reached only 0.0007 g/m²h. These results confirm the beneficial influence of samarium incorporation on the corrosion resistance of the coatings.

In order to clarify the kinetics of the corrosion processes of the four types of coatings, potentiodynamic polarization curves (PDC) of the samples in 3.5% NaCl solution were recorded. Figure 1 shows the curves with designations corre-

T a b l e 1

Results after 100 h of cyclic testing in 3.5% NaCl medium

Designations of the samples	Weight loss Δm [g/m ²] 50 h	Corrosion rate – K [g/m ² h] 50 h	Weight loss Δm [g/m ²] 100 h	Corrosion rate – K [g/m ² h] 100 h
Sm1	0.22664	0.00453	0.26441	0.00529
Sm2	0	0	0.03515	0.00070
Sm3	0.02033	0.00410	0	0
Sm4	0	0	0.12334	0.00247

sponding to the sample codes Sm1, Sm2, Sm3, and Sm4. The obtained results for the corrosion potential (E_{corr}), corrosion current density (I_{corr}), polarization resistance (R_p), and anodic (β_a) and cathodic (β_c) Tafel slopes are summarized in Table 2. Potentiodynamic polarization measurements were performed at room temperature in 3.5% NaCl using a conventional three-electrode electrochemical cell. The corrosion parameters were determined by Tafel extrapolation of the anodic and cathodic branches.

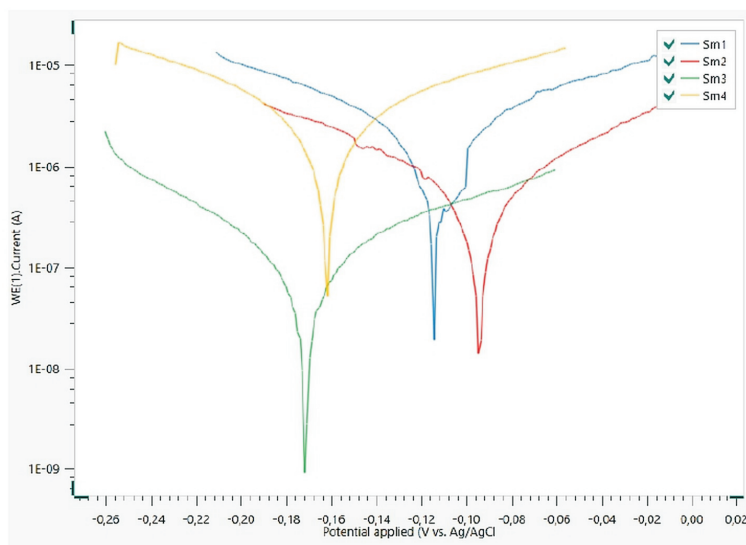


Fig. 1. Potentiodynamic polarization curves (Tafel plots) for samples Sm1, Sm2, Sm3, and Sm4

The shapes of the obtained PDCs for Sm1, Sm2, Sm3, and Sm4 indicate that uniform surface corrosion occurs in all samples. The graphs do not show a clear dominance of either the anodic or cathodic region.

From the electrochemical values presented in Table 2, it can be seen that for both types of precursors, the corrosion potential (E_{corr}) shifts slightly with in-

T a b l e 2

Potentiodynamic polarization data for samples Sm1, Sm2, Sm3, and Sm4

Sample designation	E_{corr} [V]	I_{corr} [A/cm ²]	β_a [V/dec]	β_c [v/dec]	Rp [Ω]
Sm1	-0.114	3.6299×10^{-6}	0.16281	0.156	12601
Sm2	-0.094	2.199×10^{-6}	0.27491	0.32671	30320
Sm3	-0.172	2.3902×10^{-7}	0.19992	0.12758	13551
Sm4	-0.162	2.936×10^{-5}	3.3367	0.5501	6946

creasing Sm content. For samples Sm1 (-0.114 V) and Sm2 (-0.094 V), obtained with titanium isopropoxide precursor, the corrosion potentials are higher (more noble) than those of samples Sm3 (-0.172 V) and Sm4 (-0.162 V), obtained with titanium butoxide precursor.

For the corrosion current density (I_{corr}), no direct dependence on the type of precursor or the Sm concentration was established. The lowest values of I_{corr} were obtained for samples Sm3 and Sm2, containing 0.5 at.% Sm in the titanium butoxide precursor and 1 at.% Sm in the titanium isopropoxide precursor, respectively.

The highest corrosion resistance (Rp) was measured for sample Sm2. In this case, the β_c Tafel slope is the highest, the corrosion potential E_{corr} is shifted in the most positive direction, and the polarization curve indicates improved anodic protection. Based on these results, it can be stated that the Sm2 coating provides effective protection of the steel substrate.

In contrast, the Sm4 coating (1 at.% Sm, titanium butoxide precursor) shows the lowest polarization resistance (Rp = 6946 Ω), the highest current density ($I_{\text{corr}} = 2.936 \times 10^{-5}$ A/cm²), and the largest anodic Tafel slope β_a (3.3367), indicating an accelerated anodic reaction and reduced corrosion resistance.

The results of the electrochemical corrosion tests are consistent with the gravimetric data, confirming that the best protective performance is achieved with the Sm2 coating, obtained with 1 at.% Sm and titanium isopropoxide precursor.

Surface characterization by atomic force microscopy. The prepared samples, containing different concentrations of Sm₂O₃ in either titanium isopropoxide- or titanium butoxide-based sols, were characterized by atomic force microscopy (AFM). AFM provides nanometer-scale precision in surface imaging and has become an essential technique for analyzing morphology and topography in nanotechnology and surface science. In this study, AFM imaging was employed to assess the topography and roughness of the coatings both before and after corrosion testing.

The surface area scanned was $5 \times 5 \mu\text{m}^2$, with a vertical z-range of 500 nm. The comparison of the coatings revealed differences in both morphology and roughness depending on the precursor type and the samarium concentration.

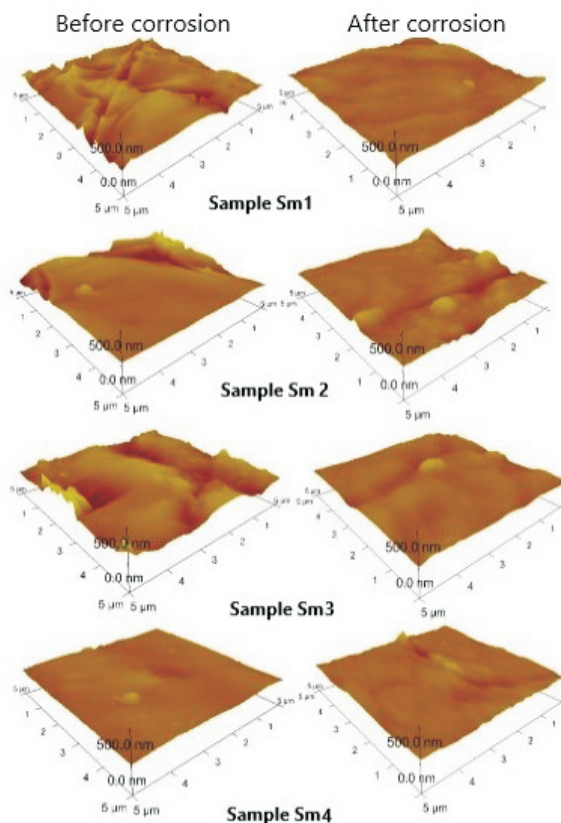


Fig. 2. 3D AFM images of the surface of samples Sm1, Sm2, Sm3, and Sm4 before and after corrosion (scan area $5 \times 5 \mu\text{m}^2$, $z = 500 \text{ nm}$)

The measured roughness values (R_a) are summarized in Table 3. Samples Sm1 and Sm3 showed a more pronounced increase in R_a after corrosion compared to samples Sm2 and Sm4. Notably, the roughness of sample Sm4 remained nearly unchanged, indicating a stable surface topography. These observations suggest that both the precursor type (titanium isopropoxide vs. titanium butoxide) and the samarium content influence the coating morphology and, consequently, the resistance to corrosion attack. In some cases, a slight decrease of R_a after corrosion exposure may occur due to the removal of weakly bonded nanoscale asperities and rounding of sharp crack edges, which results in an apparent smoothing effect without degradation of the coating integrity.

The roughness parameter R_a represents the arithmetic average of the absolute deviations (Z_j) of the surface profile from the mean plane. Lower R_a values indicate smoother surfaces and are typically associated with enhanced protective behaviour.

T a b l e 3

Roughness values of the coatings before and after corrosion testing

Samples	Sm1	Sm2	Sm3	Sm4
R _a before corrosion	45.3 nm	38.7 nm	41.8 nm	15.6 nm
R _a after corrosion	15.8 nm	20.9 nm	12.6 nm	13.2 nm

X-ray diffraction analysis. The crystalline structure of the coatings was further examined by X-ray diffraction (XRD). Figure 3 illustrates the diffraction patterns of samples Sm1 and Sm3, both containing 0.5 at.% Sm₂O₃ but synthesized from different titanium precursors: titanium isopropoxide (a) and titanium butoxide (b). The analysis revealed the presence of two crystalline phases: TiO₂ in the anatase modification and a Magnéli-type phase corresponding to non-stoichiometric titanium oxides.

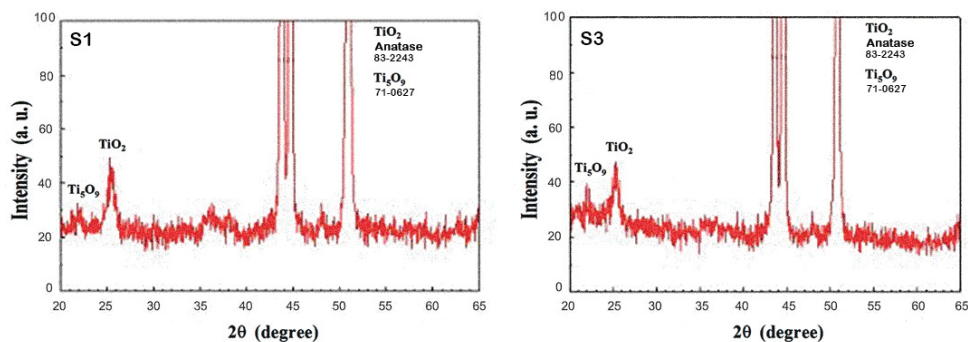


Fig. 3. XRD patterns of samples Sm1 and Sm3 (0.5 at.% Sm₂O₃) synthesized from (a) titanium isopropoxide and (b) titanium butoxide

Surface morphology after corrosion. A comparison of the coatings before and after corrosion testing showed no significant surface degradation. The surfaces remained generally smooth, with only a limited number of small pits and no detectable deposition of corrosion products. A closer examination revealed that the edges of pre-existing cracks exhibited morphological changes: before testing, the crack edges appeared sharper and more contrasting, whereas after testing they became more rounded. Importantly, no propagation or widening of cracks was observed even after 100 h of exposure (Fig. 4).

SEM observations (Fig. 4) reveal that the TiO₂/Sm₂O₃ coatings exhibit a typical sol-gel derived surface morphology. The coating surface is divided into compact domains separated by fine microcracks. This morphology is commonly attributed to shrinkage stresses during solvent evaporation, gel densification, and subsequent thermal treatment, rather than to corrosion-induced damage. Importantly, the surface inside the polygonal domains remains relatively uniform and

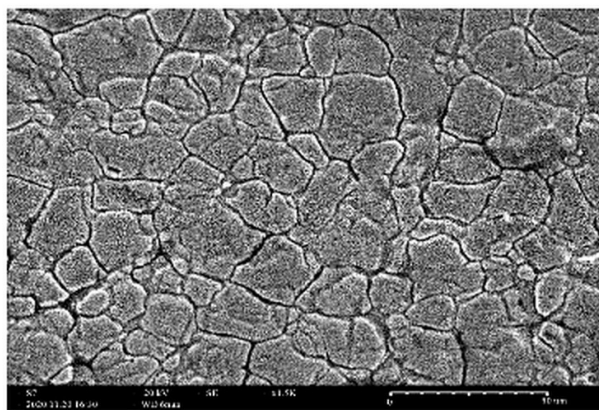


Fig. 4. SEM images of the coatings before and after 100 h cyclic corrosion testing (scale bar: 10 μm)

compact, and no deposition of corrosion products or extensive surface degradation is observed. After corrosion exposure, the crack edges appear slightly rounded; however, no widening or propagation of cracks is detected, indicating that the coating preserves its integrity and provides an effective barrier against chloride attack.

Conclusion. The combined results demonstrate that the sol-gel derived TiO_2 coatings doped with Sm_2O_3 provide an effective protective layer on 316L stainless steel substrates. The improved corrosion resistance, particularly observed for samples Sm2 and Sm3, can be attributed to the stabilizing effect of samarium ions, which modify the sol-gel network and enhance the homogeneity of the coatings. Moreover, the observed correlation between precursor type and corrosion behaviour indicates that both chemical composition and processing parameters are critical for optimizing coating performance.

Analyses confirmed that smoother surfaces with lower roughness values correspond to higher corrosion resistance, whereas increased roughness was associated with reduced protective ability. XRD results further highlighted the importance of the crystalline phases, suggesting that the presence of anatase and Magnéli-type oxides may contribute synergistically to the coatings' durability.

Overall, the study demonstrates that carefully controlled sol-gel synthesis, combined with samarium doping, leads to the formation of nanostructured TiO_2 coatings with superior protective properties, opening opportunities for their application in corrosive environments. The results further indicate that an optimal Sm content (Sm2 and Sm3) provides the best balance between structural stabilization and electrochemical protection, whereas excessive Sm (Sm4) may lead to a less protective microstructure.

REFERENCES

- [1] POPOVA K., T. PROŠEK (2022) Corrosion monitoring in atmospheric conditions: A review, *Metals*, **12**(2), 171, 1–34.
- [2] BALANGAO J. K. B. (2024) Corrosion of metals: factors, types and prevention strategies, *J. Chem. Health Risks*, **14**(1), 79–87.
- [3] POTHUMSELVI S. (2025) An overview of metal corrosion: A critical analysis, *J. Next Gener. Technol.*, **5**(5), 15–21.
- [4] SASTRI V. S., E. GHALI, M. ELBOUJDAINI (2007) *Corrosion Prevention and Protection: Practical Solutions*, New York, John Wiley & Sons, 578 pp.
- [5] SORENSEN P. A., S. KIIL, K. DAM-JOHANSEN et al. (2009) Anticorrosive coatings: A review, *J. Coat. Technol. Res.*, **6**(2), 135–176.
- [6] VESELINOV D., H. SKULEV, R. YANKOVA et al. (2023) Performance of selective plated copper coatings on stainless steel 316L and nickel alloy Ni201: microstructure, microhardness, wear resistance, and corrosion resistance, *C. R. Acad. Bulg. Sci.*, **76**(10), 1581–1590.
- [7] YANKOVA R., I. RUSEV (2025) Corrosion resistance and antifouling performance of selective plated nickel-based coatings with silver particles, *C. R. Acad. Bulg. Sci.*, **78**(3), 419–427.
- [8] FELIU S. JR., F. GARCÍA-GALVAN (2025) Corrosion and protection of metallic materials, *Metals*, **15**(4), 346, 1–8.
- [9] DUY N. D., C. T. H. HANH, N. M. HUYEN et al. (2024) Study on the application of a photocatalytic titanium dioxide coating on glass beads for the treatment of perfluorooctane sulfonic acid, *J. Chem.*, Wiley, ID 5516249, 1–14.
- [10] DINH N. N., N. T. T. OANH, P. D. LONG et al. (2003) Electrochromic properties of TiO₂ anatase thin films prepared by a dipping sol–gel method, *Thin Solid Films*, **423**(1), 70–76.
- [11] PIRDAUS N. A., N. AHMAD, F. MUHAMMAD-SUKKI et al. (2025) Effect of different titanium dioxide (TiO₂) deposition layers for dye-sensitized solar cell (DSSC) application, *Electrochim. Acta*, **527**, 146267, 1–8.
- [12] LI S., J. FU (2013) Improvement in corrosion protection properties of TiO₂ coatings by chromium doping, *Corros. Sci.*, **68**, 101–110.
- [13] YORDANOV S., I. STAMBOLOVA, L. LAKOV et al. (2018) Effect of CeO₂ dopant on the structure and protection properties of TiO₂ sprayed coatings deposited on carbon steel, *J. Chem. Technol. Metall.*, **53**(6), 1179–1185.
- [14] SAHNESARAYI M. K., H. SARPOOLAKY, S. RASTEGARI (2014) Effect of heat treatment temperature on the performance of nano-TiO₂ coating in protecting 316L stainless steel against corrosion under UV illumination and dark conditions, *Surf. Coat. Technol.*, **258**, 861–870.
- [15] PERIYASAMY A. P., M. VENKATARAMAN, D. KREMENAKOVA et al. (2020) Progress in sol-gel technology for the coatings of fabrics, *Materials*, **13**(8), 1838, 1–34.
- [16] TAN W. K., H. MUTO, G. KAWAMURA et al. (2021) Nanomaterial fabrication through the modification of sol–gel derived coatings, *Nanomaterials*, **11**(1), 181, 1–30.
- [17] KUMAR S. A., B. A. VISWANATH, P. RAGHUL (2024) A review of preparation and characterization of sol–gel coating for corrosion mitigation, *Int. J. Eng. Technol. Manag. Sci.*, **8**(2), 11–24.

- [18] GENET C., H. AZOUGAGHE, E. BRÉLIAUX et al. (2025) Multifunctional sol-gel coatings for both anticorrosion and electrical conduction properties, *Materials*, **18**(9), 2011, 1–16.

*Institute of Metal Science, Equipment and Technologies with Hydro- and Aerodynamics
Centre “Acad. A. Balevski”, Bulgarian Academy of Sciences,
67 “Shipchenski Prohod” Blvd, 1574 Sofia, Bulgaria
e-mails: stancho14@abv.bg, b_jiv@abv.bg, vladimir2pe@yahoo.com,
joanna_hristova@abv.bg, v_diakova@ims.bas.bg,
mihaelaaleksandrova204@gmail.com, shaban_uzun@abv.bg*